Journal of Numerical Thanatochronometry

Received 29 March 2021; accepted 1 November 2021
Date of current version 15 November 2021
Digital Object Identifier: pending

Approximation of Antemortem Axial Temperature Distribution for Death-time Estimation

Sipho Mfolozi[1]

***Abstract*— Preliminary investigations suggest that antemortem axial temperature distribution in a body predicts the character of postmortem cooling by causing presence/absence of the postmortem temperature plateau. Antemortem axial temperature distribution is thus a less appreciated source of uncertainty in death-time estimation. Empiric methods of thermometric death-time estimation apply a 37°C single-point (rectal) approximation to represent antemortem body temperature. Numerical methods of death-time estimation apply 3D human phantoms of often relatively low anatomical segmentation, as well as varying bioheat techniques when approximating antemortem temperature distribution. Often, simulation of postmortem cooling used to estimate the death interval is conducted in continuity with approximation of antemortem body temperature distribution. This paper proposes separation of approximation of antemortem temperature distribution by using a high-definition 3D human computational phantom with 247 anatomically segmented organs, by applying the Pennes bioheat model, and by applying metabolic heat-generation and blood perfusion rates as additional organ parameters. Results indicated that the approximated antemortem temperature was inhomogeneous, with wide temperature variations documented on the skin. The approximated axial temperature varied according to location, size, shape and metabolic rate of organs in a given axial section. Regions of heart muscle, kidneys and extra-pelvic muscles showed high temperatures in axial planes of the chest, abdomen and pelvis, respectively. Axial temperature transition from the body core to skin was nonlinear. This paper proposes approximation of the antemortem physical exertion from death scene investigation, determination of its metabolic equivalent value, and proportional distribution to exertion-involved organs.**

***Keywords* —** axial temperature distribution, PMTP, numerical approximation, death-time estimation, 3D phantom

I. Introduction

A study in 2013 indicated that the axial temperature distribution in a body at death predicted the character of postmortem cooling [1]. The rate of cooling of the body core immediately after death was observed to depend on the temperature of the body bulk around it, and not directly on the temperature of the ambient air. This relationship was less obvious because empiric methods of death-time estimation, such as Marshall and Hoare's Cooling Formula [2] and the Henβge Rectal Temperature Nomogram method [3] – [6], applied a rectal temperature measurement from a body found dead together with the temperature value of ambient air, but did not explicitly require approximation of antemortem axial temperature distribution. The 2013 study indicated that the cooling curve of a body whose core temperature was 37°C at death exhibited a postmortem temperature plateau (PMTP) only when temperature of the body-bulk around the core was also 37°C at death. However, the cooling curve did not exhibit a PMTP when temperatures of the core and body-bulk at death were 37°C and ~15°C, respectively, even though ambient air temperatures were identical in both scenarios. The PMTP is a period after death during which the core temperature remains unchanged for a variable time. It is a phenomenon observed in many postmortem studies, whose causes were debated by numerous authors [2], [4] – [22] without consensus. The fact that core temperatures at death were identical in the two postmortem cooling scenarios, along with ambient air temperatures that hadn't been altered, suggested that application of an antemortem rectal temperature approximation of 37°C in death-time estimation by empiric methods may be a source of uncertainty. The suggestion was that the antemortem axial temperature distribution, now proven to be a predictor of the PMTP, should perhaps be the variable that is approximated for death-time estimation. After all, the second exponential term in Marshall and Hoare's Cooling Formula represented the PMTP, whose method of quantification for a body found dead unfortunately never came to be described. The Cooling Formula was the foundation on which the Henβge Rectal Temperature Nomogram method was developed.

[1]Department of Forensic Medicine, University of KwaZulu-Natal, Durban 4000, South Africa
Email: sipho.mfolozi@gmail.com

A – Approximation of antemortem body temperature by empiric methods of death-time estimation

Erstwhile authors such as Schwarz and Heidenwolf [9] noted the effects of antemortem body temperature on the effect of subsequent body cooling. Al-Alousi [23] [24]also emphasised the significance of accurate approximation of antemortem body temperature in relation to his microwave thermometry method of death-time estimation. Al-Alousi suggested averaging of temperature values at death to be used for the brain, liver, and rectum (naked and covered) based from their results. Some authors excluded cases whose body temperatures before death were outside normal parameters [25], without elaborating.

The antemortem body temperature value applied in the Cooling Formula and the Rectal Temperature Nomogram Method is a single-point approximation of antemortem temperature of the rectum at death, whose value is 37°C. In these methods, the 37°C antemortem rectal temperature is regarded as a representation of body-core temperature. Antemortem core temperature, on the other hand, is regarded as more reliable representation of total-body temperature for purposes of death-time estimation as it is less likely to be affected by ambient fluctuations. The Cooling Formula and the Rectal Temperature Nomogram Method do not approximate the antemortem axial temperature distribution of a body found dead.

B - Approximation of antemortem body temperature by numerical methods of death-time estimation

Numerical methods of death-time estimation apply a 3D geometry that represents the body found dead. The nature of numerical analysis of heat transfer requires temperature of the 3D geometry under consideration – referred to as the initial condition – to be defined. Various strategies of defining the initial condition are employed by the different numerical methods of death-time estimation. For example, in the heat-flow Finite Element Model (FEM) [26] [27], the temperature distribution of the skin of the 3D geometry was approximated from 37°C by linear gradient down to 27°C on the surface layers of the distant extremities. The FEM approximated antemortem temperature distribution of internal viscera by converting the approximated basal metabolic rate related to body mass into a power-density value – 60% of it was apportioned to the body core (mediastinum, lungs, upper abdominal organs, gastrointestinal organs, kidneys and pelvic organs); 18% to the muscle compartment; 17% to the brain and 5% to bone and connective tissues of the face and neck. The numerical analysis method by Schenkl et al. [28] applied a second-order homogeneous partial differential equation to define the initial temperature field of their CT-derived 3D human geometry at death. Weiser et al. [29] approximated the initial temperature field of the CT-derived 3D human geometry by using the Pennes bioheat equation, without providing further information about the resultant temperature field. The numerical method of death-time estimation by Wilk et al. [30] assigned a uniform initial body temperature of 37°C to the 3D computational phantom. Variations in methods of approximating the antemortem temperature distribution present a source of uncertainty in death-time estimation.

C – Anatomical fidelity of 3D computational geometries used by numerical methods of death-time estimation

There is inconsistency in anatomical fidelity of 3D computational geometries used by various numerical methods of death-time estimation. For example, the 3D geometry used by Wilk et al consisted of cones representing arms and legs, an ellipsoid representing the head, and cylinders representing the neck and torso. Proportions of these basic shapes were dictated by standardised anatomical measurements. The Wilk 3D geometry [30] consisted of compartments representing fat, non-adipose tissue and substrate. The CT-derived 3D computational geometry used by Schenkl et al [28] and by Weiser at al [29] consisted of 14 tissue compartments. The FEM 3D geometry used by Mall and Eisenmenger [26] [27] was a humanoid that consisted of 8328 solid cuboidal elements and 10154 nodes. The number of elements and nodes increased with inclusion of the ground surface. The FEM 3D geometry also consisted of 14 tissue compartments that approximated the morphology and location of internal viscera. Inconsistency in anatomical fidelity among numerical methods presents a source of uncertainty in death-time estimation.

II. MATERIALS

A – A high fidelity 3D computational human phantom

This study applied a high-resolution 3D computational human phantom of an adult male part of a larger collection of computational phantoms known as the version 3.0 Virtual Population [31], which were sourced from the IT'IS Foundation, Switzerland (https://itis.swiss/virtual-population/virtual-population/vip3/). The Virtual Population 3D computational human phantoms were each given a name and covered a wide anthropometric range, consisting of males, females, adults, young children, prepubescent children, infants, a pregnant female at different gestational ages, an elderly male, and an obese adult male.

The 3D computational human phantom chosen for this study (named Duke) was built from full-body magnetic resonance images (MRIs) of a healthy living subject and consisted of 247 anatomically segmented organs that included non-tissue constituents such as urine, respiratory tract air, bile, and gastrointestinal contents – all of which

are present in the human body in life and therefore had to be included in the approximation of antemortem axial body temperature distribution. The living subject from which the phantom was built was 34 years old, 1.77m tall and weighed 70.2kg.

Virtual Population 3D computational phantoms were verified either individually or as selected groups by a number of studies. For example, Farcito et al. [32] provided an assessment of MRI image segmentation quality and processes by anatomical experts. Gosselin et al. [31] described assessment of the fidelity of extracted surfaces and simplified surfaces of the 3D computational phantoms. Liorni et al. [33] proposed a novel method and procedure for evaluating compliance of sources with strong gradient magnetic fields, such as wireless power transfer systems, which mitigates overestimation of human exposure while maintaining simplicity of the testing procedure using the phantoms Duke, Billie, Nina and Fats. Nadakuduti et al. [34] described a compliance testing methodology for wireless power transfer systems using the four such high-fidelity 3D computational phantoms. Kyriakou et al. [35] applied the chosen adult male phantom's head to model full-wave acoustic and thermal transcranial ultrasound propagation. Murbach et al. [36] modelled radio frequency exposure on pregnant female 3D computational phantoms.

B – Thermal analysis software

The thermodynamic solver used in this study was known as P-Thermal®. It was an integral part of a larger bio-physics simulation platform called Sim4Life® [37] from Zurich MedTech, Switzerland (https://zmt.swiss/sim4life/). The P-Thermal® solver was based on Poisson differential equation and enabled modelling of heat transfer in living tissue with a set of flexible boundary conditions. Validation of the P-Thermal® solver [38] consisted of theoretical solutions and corresponding simulation results of four scenarios.

The P-Thermal® solver was verified in experimental studies by comparison with analytically solvable cases, experimental measurements under controlled conditions and *in vivo* measurements. For example, Murbach et al. [39] demonstrated the application of the P-Thermal® solver in modelling magnetic resonance imaging (MRI) radiofrequency (RF)-exposure induced tissue heating for safety assessment, considering local thermoregulation by vasodilation. They provided comparison against in *vivo* measurements and provided detailed uncertainty assessment considerations. In another verification study, Neufeld et al. [40] applied the P-Thermal® solver to the investigation of RF-exposure related to heating in the presence of implants, with a particular focus on wires and leads. In that study, a thin structure model, previously verified by Neufeld [41] was used to facilitate the modelling of setups featuring thin, highly thermo-conductive wires. That verification study also provided detailed uncertainty assessment considerations. The staircasing-effect correction approach used in the P-Thermal® solver and its implantation was verified by Neufeld et al. [42].

Other studies that verified the P-Thermal® solver include design and optimization of ultrasonic therapy [35], assessment of medical device safety in MRI [43], RF-hyperthermia liver tumour treatment simulation [44], prediction of tumour temperature in regional hyperthermia by using LED luminance [45], temperature impact on neuronal dynamics [46] and other studies. The transient thermal solver of the P-Thermal® solver assumed that a transient state existed in the 3D computational phantom, which required all tissue domains to have non-zero thermal conductivity or non-zero heat transfer rates.

C – Computer hardware

Simulations were carried out in a 2015-model Apple Mac Pro computer that had a 12-core 3.5GHz processor, a 128GB RAM and ran 64-bit Windows 8.1-10. Simulation data were stored in a 10TB external hard drive.

III. METHODS

A – BioHeat modelling

The finite difference time domain (FDTD) method was applied in this study to approximate antemortem temperature distribution in the chosen 3D computational human model. The numerical simulation type was transient / unsteady-state, and the bioheat model used was the Pennes bioheat model [47], which can be expressed as:

$$\rho_t C_t \frac{\partial T_{ti}}{\partial t} = \nabla \cdot (k_t \nabla T_{ti}) + \rho_b C_b \omega_b (T_b - T_{ti}) + Q_m \quad (1)$$

where ρ_t was density of an organ, C_t was the specific heat capacity of an organ, t was time, k_{ti} was thermal conductivity of an organ, ρ_{bl} was density of blood, C_{bl} was the specific heat capacity of blood, ω_b was the blood perfusion rate of an organ, T_b was the convective temperature of blood, T_{ti} was temperature of an organ and Q_m was the metabolic-heat generation rate of an organ. The Pennes bioheat equation (PBE) was simultaneously applied to the 247 organs of the chosen 3D computational

human phantom. Each organ's Q_m constituted a continuous heat source that was assumed to be spatially homogeneous. Heat generated by each organ was spread to adjacent organs by thermal diffusion as well as blood perfusion, whose mathematical representation acted as a homogeneous, organ-specific heat-sink term. The combined effects of simulated endogenous metabolic heat, heat transfer by blood flow, heat transfer between organs by thermal conduction, and heat transfer between the skin and ambient air by thermal convection and thermal radiation determined the overall temperature filed of the 3D computational human phantom.

Variables ρ_t, C_t, and k_{ti} in eqn. (1) were standard tissue parameters that the previously discussed numerical methods of death-time estimation applied. This study applied additional specified variables Q_m and ω_b, representing a tissue's metabolic heat generation rate and its blood perfusion rate, respectively.

B – Initial condition

Any numerical simulation requires an initial condition, even when the purpose is to approximate antemortem body temperature distribution. Any temperature value applied would have no impact on accuracy of the solution. The chosen initial condition for this study was 37°C.

C – Boundary condition

On the skin, boundary conditions that specified the thermal conditions were applied, namely the Dirichlet (far field air has a fixed temperature), Neumann (heat transfer from body to air is purely due to a heat transfer coefficient), and 'mixed' (Dirichlet plus Neumann) boundary conditions. In a mixed boundary condition, the convective heat flux is the product of the heat transfer coefficient and local temperature difference between skin and air temperatures. Mixed boundary condition work well for modelling effects of stagnant convection, i.e. in the absence of wind and natural convection. In a mixed boundary condition, the convective heat flux is the product of the heat transfer coefficient (e.g. radiative heat flux) and local temperature difference between skin and air temperatures. A mixed boundary condition is expressed mathematically as:

$$\frac{kdT_s}{dn} + h(T_s - T_a) = F_{Boundary} \quad (2)$$

where T_s represented skin temperature, T_a represented air ambient temperature, n is the unit normal, k is a constant, and h represented the heat transfer coefficient. Exchange of the radiative heat is derived from the Stefan-Boltzmann equation, in the form:

$$\sigma(T_s^4 - T_a^4) \quad (3)$$

where σ represented the Stefan-Boltzmann constant (5.670373×10^{-8} Wm^{-2} K^{-4}). Eqn. 3 can be expressed as:

$$\sigma(T_s^4 - T_a^4) = (T_s - T_a)(T_s + T_a)(T_s^2 + T_a^2) \quad (4)$$

For small temperature differences, eqn. 4 can be approximated as:

$$4\sigma(T_s - T_a)T_a^3 \quad (5)$$

and prescribed as part of the mixed boundary condition as:

$$h = 4\sigma T_a^3 \quad (6)$$

The heat transfer coefficient h applied in this study was 3.4 $Wm^{-2}°C^{-1}$ [48] and the air temperature T_a was set to 22°C.

D – Organ Parameters

Values of all the variables applied in eqn. (1) were obtained from the IT'IS Foundation [49]. The 3D computational human phantom consisted of non-thermogenic organs whose Q_m and ω_b values were zero by default, viz. air, bile, blood, bronchi lumen, cerebrospinal fluid, cornea, lens, oesophagus lumen, non-infiltrated fat, heart lumen, large intestine lumen, pharynx, small intestine lumen, stomach lumen, trachea lumen, tooth and vitreous humour. The calculated sum of mean Q_m of all the phantom's organs was 154W, which was the metabolic equivalent of a 70kg individual jogging on level ground at 9 km/hr [50].

E – Grid Design

Discretization to transform the 3D computational human phantom to a rectilinear mesh was performed using Sim4Life®'s rectilinear non-uniform gridding algorithm, which used ray-tracing and robust intersection testing, identified relevant structural features of the 3D computational phantom and then suggested a Cartesian grid that could neatly and properly resolve it. This ensured mesh-independent solutions. The grid refinement level applied was 'normal' (others were 'course', 'fine' and 'very fine'). The resolution of 3D computational phantoms was 10mm in the *xyz* axes. The final grid consisted of 3.4595×10^7 cells.

IV. RESULT

A – Approximated skin temperature distribution

The simulation interval required to produce a stable solution in this study was not known in advance but was established through trial and error to be 9000 seconds. The approximated temperature fields of all organs showed spatial inhomogeneity, varying in the *xyz* coordinates. The predicted inhomogeneity was also demonstrated on the skin of the 3D computational human phantom, consistent with observations using infrared thermography [51]. Fig. 1 indicates the approximated antemortem skin temperature distribution, which ranged from 20.6°C to 41°C. Quantitative comparison with skin temperature distribution reported in the literature could not be conducted due to variations in physical exertion, ambient temperature, skin moisture, clothing and prevailing thermoregulatory mechanisms. However, human skin temperature in air during exercise on a treadmill and at rest is also known to be inhomogeneously distributed [52].

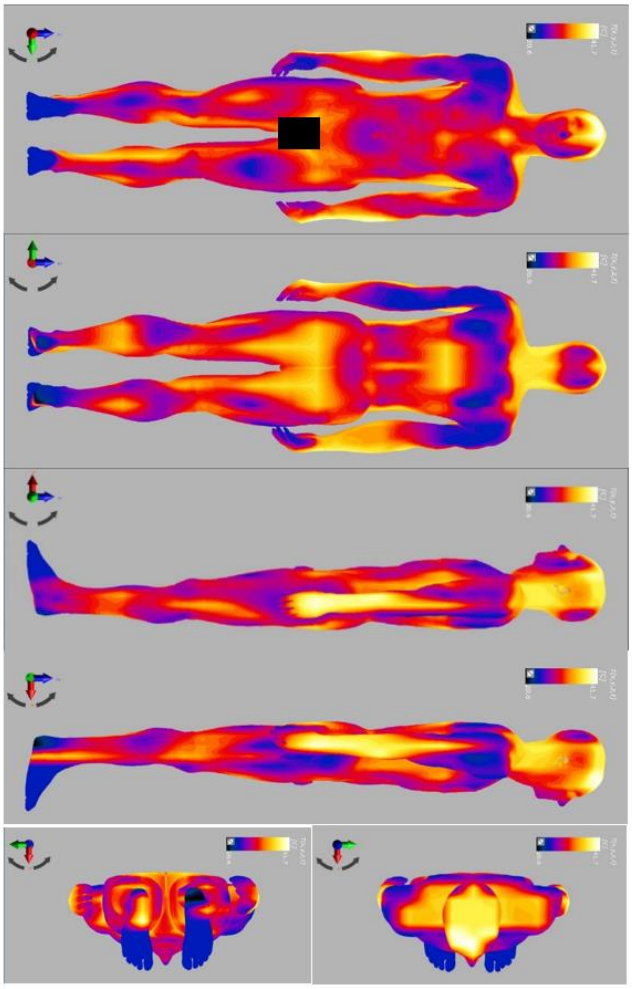

Fig.1 Approximated antemortem skin temperature distribution of the chosen 3D computational human phantom with a metabolic equivalent of 154W at 22°C air.

B – Approximated axial temperature distribution

Axial sections of the approximated antemortem body temperature were consistent with the generally accepted notion that that the living human body consists of a cooler 'outer shell' and a 'hot core'. The location and size of the antemortem central isotherm (ACI) (hot core) at a given axial section appeared to be determined by the location, shape, and size of an organ with a high relative Q_m value, among other parameters. For example, at the level of the chest (1327mm from the ground), the heart muscle exhibited an isotherm of highest temperature while blood in the heart chamber and descending thoracic aorta (both of which represent blood that is a heat-sink term in the PBE) indicated isotherms of lowest temperature (see Fig. 2). The axial temperature profile through the chest was non-linear and varied according to whether the coronal (yz) or the sagittal/parasagittal (xz) plane was selected for examination. Fig. 3 indicates 1D axial temperature curves of the chest plotted from various planes.

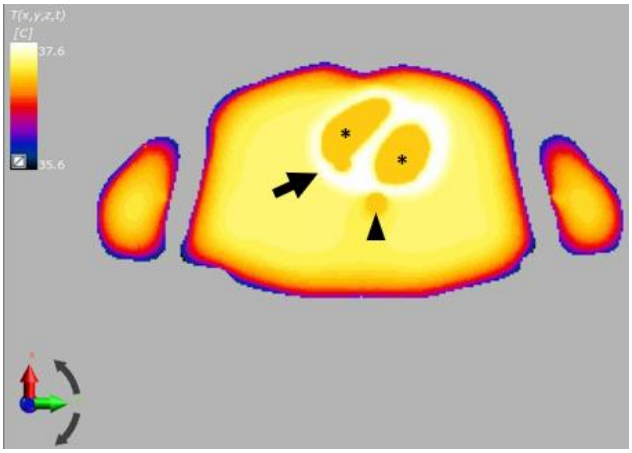

Fig. 2 Approximated antemortem axial temperature distribution at the chest level. The arrow indicates the 'heart muscle' isotherm, the arrowhead indicates the 'descending thoracic aorta lumen (blood)' isotherm and the Asterix indicate 'heart lumen (blood)'. The oval shapes on either side of the chest are isotherms of the arms.

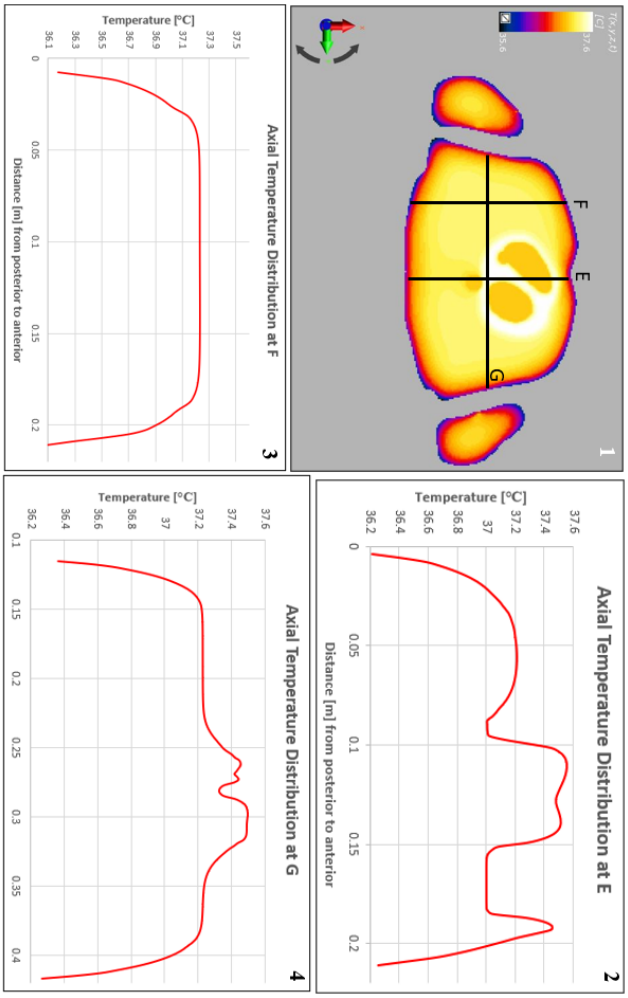

Fig. 3 One-dimensional curves of approximated antemortem axial temperature distribution of the chest obtained at various planes. Image 1 indicates three selected planes. Image 2 indicates the 1D temperature curve obtained from plane E.. Image 3 indicates the 1D temperature curve obtained from plane F. Image 4 indicates the 1D temperature curve obtained from plane G.

At the level of the abdomen (1091mm from the ground), the kidneys exhibited symmetrical posteriorly positioned isotherms of highest temperature (Fig. 4). The 1-dimensional axial temperature profile in the abdomen also varied according to the chosen coronal, sagittal or parasagittal plane of examination, as indicated in Fig. 5.

At the level of the pelvis where the 3D computational phantom's rectosigmoid junction was located (the position of rectal thermometry), skeletal muscles outside of the pelvic girdle formed symmetrical isotherms of the highest temperature (Fig. 6). There too, the 1-dimensional axial temperature profile varied according to the chosen coronal, sagittal or parasagittal plane of examination, as indicated in Fig. 7.

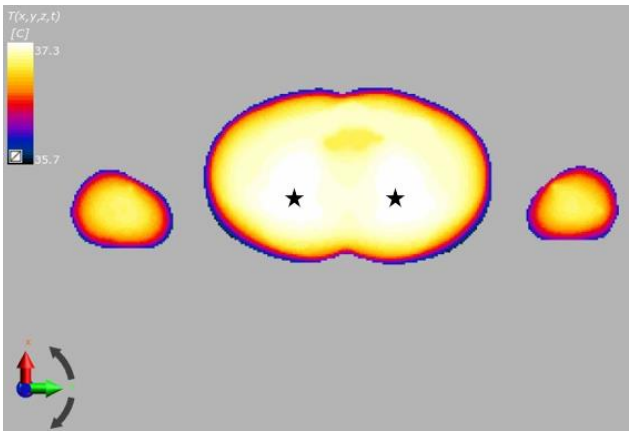

Fig. 4 Approximated antemortem axial temperature distribution at the abdomen level. Stars indicate 'kidney' isotherms. The oval shapes on either side of the abdomen are isotherms of the arms.

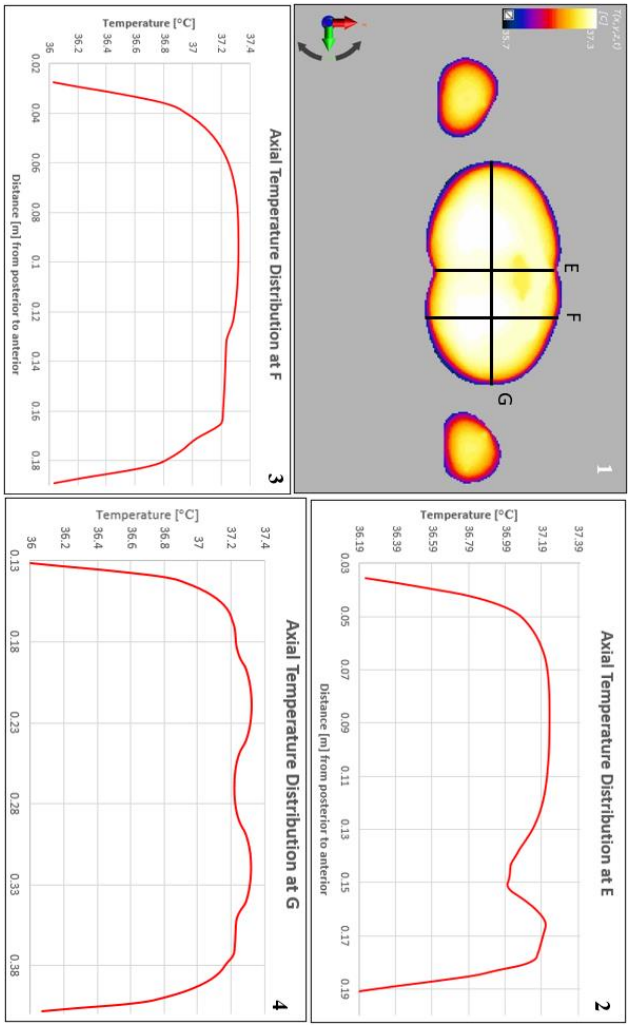

Fig. 5 One-dimensional curves of approximated antemortem axial temperature distribution of the abdomen obtained at various planes. Image 1 indicates three selected planes. Image 2 indicates the 1D temperature curve obtained from plane E.. Image 3 indicates the 1D temperature curve obtained from plane F. Image 4 indicates the 1D temperature curve obtained from plane G.

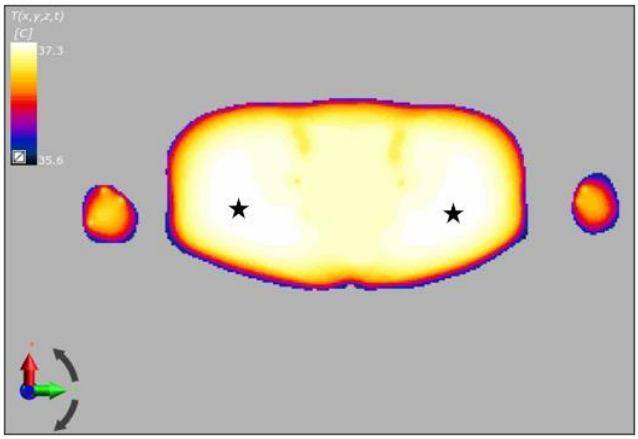

Fig 6 Approximated antemortem axial temperature distribution at the pelvis level. Stars indicate 'skeletal muscle' isotherms outside the pelvic girdle. The oval shapes on either side of the chest are isotherms of the forearms.

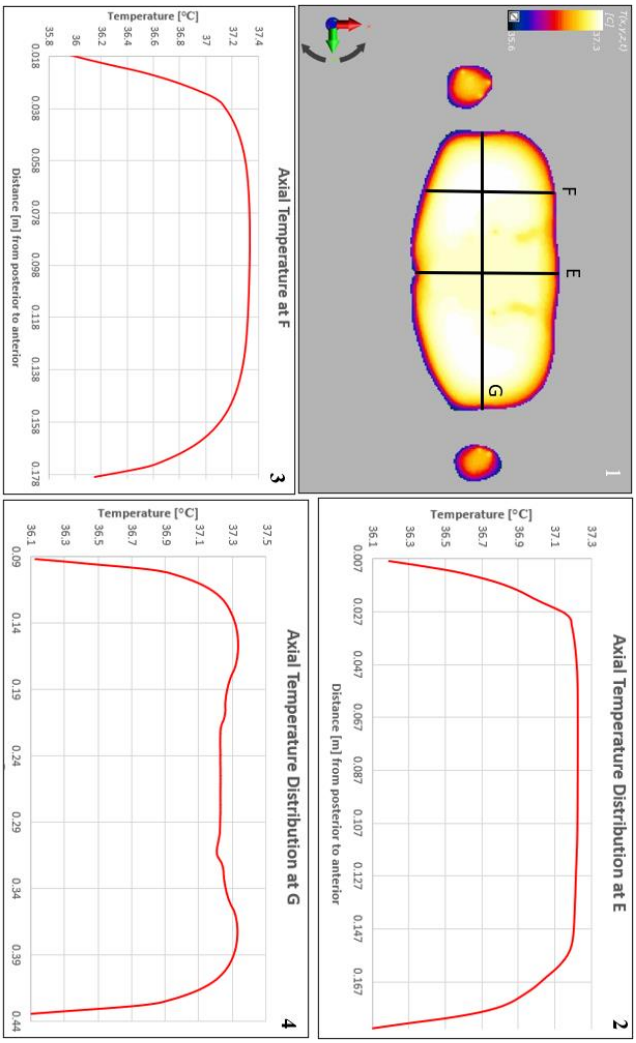

Fig. 7 One-dimensional curves of approximated antemortem axial temperature distribution of the pelvis obtained at various planes. Image 1 indicates three selected planes. Image 2 indicates the 1D temperature curve obtained from plane E.. Image 3 indicates the 1D temperature curve obtained from plane F. Image 4 indicates the 1D temperature curve obtained from plane G.

The approximated axial temperature distribution showed a similar profile in all parts of the body when plotted as a curve. The ACI occupied a significant proportion of the body circumference, appearing as the flat part of temperature curve, while cooler subcutaneous and skin temperatures formed the slopes on either side.

CONCLUSION

This study demonstrated application of high anatomical-fidelity 3D human phantoms for numerical approximation of antemortem axial temperature distribution, both for understanding its relationship with postmortem cooling and for death-time estimation. The Pennes BioHeat Model allows application of the additional, tissue-specific parameters Q_m and ω_b, which may be adjusted to simulate a decedent's antemortem state of physical activity according to death-scene investigation. As stated earlier, the axial temperature distribution in a body at death is thought to be a predictor of the character of postmortem cooling. The manner in which it does so, however, is beyond the scope of this paper and requires a separate investigation. Numerical approximating the antemortem axial temperature distribution demonstrated in this paper is the first step towards that understanding. A follow-up study would be to demonstrate the character of postmortem axial heat transfer commencing from such an approximation, in which Q_m and ω_b may simply be assigned zero values to simulate death.

ACKNOWLEDGEMENTS

The research was funded by the National Research Foundation (NRF) of South Africa under the Thuthuka PhD Track funding instrument, fund number TK14042966700. Sim4Life®, the biological simulation software that includes a thermal solver, was generously provided by Zurich MedTech, Switzerland. The 3D computational phantoms were generously provided by IT'IS Foundation, Switzerland. I acknowledge contributions by Professors AG Malan, T Bello-Ochende and LJ Martin of the University of Cape Town, South Africa.

REFERENCES

[1] S. Mfolozi, *Cooling rates of dummies under various degrees of air humidity, wind speed and air temperature*, Cape Town, 2013.

[2] T. Marshal and F. Hoare, "Estimating the time of death. The rectal cooling after death and its mathematical expression," *Journal of Forensic Science*, vol. 7, pp. 56-81, 1962.

[3] C. Henβge, "Die Prazision von Todeszeitchatzungen durch die mathematische Beschriebung der rektalen Leichenbkuhlung (Precision of estimating the time of death by mathematical

expression of rectal body cooling. German, summary in English)," *Zeit. Rechtsmed,* vol. 83, pp. 45-67, 1979.

[4] C. Henβge, "Temperatur-Todeszeit-Nomogramm für Bezugsstandardbedingungen der Leichenlagerung (Temperature-death-time nomogram for reference to standard conditions of cadaver storage. German, abstract in English)," *Krim. Forensische Wiss.,* pp. 109-115, 1982.

[5] C. Henβge, "Death time estimation in case work. I. The rectal temperature time of death nomogram," *Forensic Science International,* vol. 38, no. 3-4, pp. 209-236, 1988.

[6] C. Henβge, "Rectal temperature time of death nomogram: Dependence of corrective factors on body weight under stronger thermic insulation conditions," *Forensic Science International,* vol. 54, no. 1, pp. 51-66, 1992.

[7] J. Davey, "Observations on the temperature of the human body after death," *Researches, Physiological and Anatomical,* pp. 323-330, 1839.

[8] H. Rainy, "On the cooling of dead bodies as indicating of length of time that has elapsed since death," *Glasgow Medical Journal,* vol. 1, no. 3, pp. 323-330, 1869.

[9] F. Schwarz and H. Heidenwolf, "Postmortem cooling and its relation to the time of death," *International Criminal Police Review,* pp. 339-344, December 1953.

[10] H. Shapiro, "Medicolegal mythology: Some pupular forensic falacies," *Journal of Forensic Medicine,* vol. 1, no. 3, pp. 144-159, 1954.

[11] G. De Saram, G. Webster and N. Kathirgamatamby, "Postmortem temperature and the time of death," *Journal of Criminal Law and Criminology,* vol. 46, no. 4, pp. 562-577, 1955.

[12] H. Lyle and F. Cleveland, "Determination of the time of death by heat loss," *Journal of Forensic Science,* vol. 1, no. 4, pp. 11-24, 1956.

[13] F. Lundquist, "Physical and chemical methods for the estimation of the time of death," *Acta Medicinae Legalis et Socialis,* vol. 9, pp. 205-213, 1956.

[14] A. Joseph and E. Schickele, "A general method for assessing factors controlling postmortem cooling," *Journal of Forensic Science,* vol. 15, no. 3, pp. 364-391, 1970.

[15] A. Brown and T. Marshall, "Body temperature as a means of estimating time of death," *Forensic Science International,* vol. 4, pp. 125-133, 1974.

[16] B. Brinkmann, D. May and U. Riemann, "Postmortaler Temperaturausgleich im Bereich des Kopfes. I. Meβtechnik, prinzipielle Untersuchungen. (Postmortem temperature compensation in the area of the head. I. Measuring technique, principal investigations. German, summary in English)," *International Journal of Legal Medicine,* vol. 78, pp. 69-82, 1976.

[17] B. Brinkmann, G. Menzel and U. Riemann, "Postmortale Organtemperaturen unter verschiedenen Umweltbedingungen. (Postmortem organ temperatures under different environmental conditions. German, summary in English)," *International Journal of Legal Medicine,,* vol. 81, pp. 207-216, 1978.

[18] L. Nokes, B. Hicks and B. Knight, "The post-mortem temperature plateau—fact or fiction?," *Med. Sci. Law,* vol. 25, no. 4, pp. 263-264, 1985.

[19] L. Althaus and C. Henβge, "Rectal temperature time of death nomogram: sudden change of ambient temperature," *Forensic Science International,* vol. 99, no. 3, pp. 171-178, 1999.

[20] P. Bisegna, C. Henβge, L. Althaus and G. Giusti, "Estimation of the time since death: Sudden increase of ambient temperature," *Forensic Science International,* vol. 176, no. 2-3, pp. 196-199, 2008.

[21] J. Smart, "Estimation of the time of death with a Fourier series unsteady-state heat transfer model," *Journal of Forensic Science,* vol. 55, no. 6, pp. 1481-1487, 2010.

[22] J. Smart and M. Kaliszan, "The post-mortem temperature plateau and its role in the estimation of time of death. A review," *Legal Medicine,* vol. 14, no. 2, pp. 55-62, 2012.

[23] L. Al-Alousi and R. Anderson, "Microwave thermography in forensic medicine," *Police Surgeon,* vol. 30, pp. 30-42, 1986.

[24] L. Al-Alousi, R. Anderson and D. Land, "A non-invasive method for postmortem temperature measurements using a microwave probe," *Forensic Science International,* vol. 64, no. 1, pp. 34-46, 1994.

[25] F. Fiddes and T. Patten, "A percentage method for representing the fall in body temperature after death: its use in estimating the time of death," *Journal of Forensic Medicine,* vol. 5, pp. 2-15, 1958.

[26] G. Mall and W. Eisenmenger, "Estimation of time since death by heat-flow Finite-element model part I: method, model, calibration and validation," *Legal Medicine,* vol. 7, no. 1, pp. 1-14, 2005.

[27] G. Mall and W. Eisenmenger, "Estimation of time since death by heat-flow Finite-element model part II: application to non-standard cooling conditions and preliminary results in practical casework.," *Legal Medicine,* vol. 7, no. 2, pp. 69-80, 2005.

[28] S. Schenkl, H. Muggenthaler, M. Hubig, B. Erdmann, M. Weiser, S. Zachow, A. Heinrich, F. Güttler, U. Teichgräber and G. Mall, "Automatic CT-based finite element model generation for temperature-based death time estimation: feasibility study and sensitivity analysis," *International Journal of Legal Medicine,* vol. 131, pp. 699-712, 2017.

[29] M. Weiser, B. Erdmann, S. Schenkl, H. Muggenthaler, M. Hubig, G. Mall and S. Zachow, "Uncertainty in temperature-based determination of time of death," *Heat and Mass Transfer,,* vol. 54, pp. 2815-2826, 2017.

[30] L. Wilk, R. Hoveling, G. Edelman, H. Hardy, S. van Schouwen, H. van Venrooij and M. Aalders, "Reconstructing the time since death

using non-invasive thermometry and numerical analysis," *Science Advances*, vol. 6, no. 24, pp. 1-7, 2020.

[31] M. Gosselin, E. Neufeld, H. Moser, E. Huber, S. Farcito, L. Gerber, M. Jedensjö, I. Hilber, F. Di Gennaro, B. Lloyd, E. Cherubini, D. Szvzerba, W. Kainz and N. Kuster, "Development of a new generation of high-resolution anatomical models for medical device evaluation: the Virtual Population 3.0," *Physics in Medicine and Biology*, vol. 59, no. 18, pp. 5287-5303, 2014.

[32] Farcito, S; Lloyd, B; Kuster, N;, "Verification Report VIP001AA201704: Virtual population models V3.x verification of anatomy, physiology and segmentation/generation procedures," IT'IS Foundation, Zurich, 2017.

[33] I. Liorni, T. Lisewski, M. Capstick, S. Kühn, E. Neufeld and N. Kuster, "Novel method and procedure for evaluating compliance of sources with strong gradient magnetic fields such as wireless power transfer systems," *IEEE Transactions on Electromagnetic Compatibility*, vol. 56, no. 5, pp. 1027-1034, 2019.

[34] J. Nadakuduti, M. Douglas, L. Lu, A. Christ, P. Guckian and N. Kuster, "Compliance testing methodology for wireless power transfer systems," *IEEE Transactions on Power Electronics* , vol. PP, no. 99, pp. 1-1, 2015.

[35] A. Kyriakou, E. Neufeld, B. Werner, G. Székely and N. Kuster, "Full-wave acoustic and thermal modeling of transcranial ultrasound propagation and investigation of skull-induced aberration correction techniques: a feasibility study," *Journal of Therapeutic Ultrasound*, vol. 3, no. 11, pp. 1-18, 2015.

[36] M. Murbach, E. Neufeld, T. Samaras, J. Córcoles, F. Robb, W. Kainz and N. Kuster, "Pregnant women models analyzed for RF exposure and temperature increase in 3T RF shimmed birdcages," *Magnetic Resonance in Medicine*, vol. 77, no. 5, pp. 2048-2056, 2017.

[37] ZMT Zurich MedTech AG, "Sim4Life Documentation Release 5.2," Zurich Medical Technology, Zurich, 2020.

[38] Szolnoki, L; Neufeld, E; Kuster, N;, "Sim4Life and SEMCAD Thermal Solver (Verification Report TS002AA201812)," Foundation for Research on Information Technologies in Society, 2018.

[39] M. Murbach, E. Neufeld, M. Capstick, W. Kainz, D. Brunner, T. Samaras, K. Pruessmann and N. Kuster, "Thermal tissue damage model analyzed for different whole-body SAR and scan durations for standard MR body coils," *Magnetic Resonance Medicine*, vol. 71, no. 1, pp. 421-431, 2013.

[40] E. Neufeld, S. Kühn, G. Szekely and N. Kuster, "Measurement, simulation and uncertainty assessment of implant heating during MRI," *Phys. Med. Biol.*, vol. 54, no. 13, pp. 4151-4169, 2009.

[41] E. Neufeld, "High resolution hyperthermia treatment planning. PhD Thesis.," Swiss Federal Institute of Technology, Zurich, 2008.

[42] E. Neufeld, N. Chavannes, T. Samaras and N. Kuster, "Novel conformal technique to reduce staircasing artifacts at material boundaries for FDTD modeling of the bioheat equation," *Phys. Med. Biol.*, vol. 52, no. 15, p. 4371, 200

[43] J. Kabil, L. Belguerras, S. Trattning, C. Pasuier, J. Felblinger and A. Missoffe, "A Review of Numerical Simulation and Analytical Modeling for Medical Devices Safety in MRI," *Yearb Med Inform*, vol. 10, no. 1, pp. 152-158, 2016.

[44] B. Prasad, Y. Ha, S. Lee and J. Kim, "Patient-specific simulation for selective liver tumor treatment with noninvasive radiofrequency hyperthermia," *Journal of Mechanical Science and Technology*, vol. 30, no. 12, pp. 5837-5845, 2016.

[45] J. Lee, Y. Seol, T. Oh, N. An, K. Han, J. Hwang, H. Jang, B. Choi and Y. Kang, "Prediction of Tumor Temperature in Regional Hyperthermia by Using LED Luminance," *Journal of the Korean Physical Society*, vol. 77, pp. 524-529, 2020.

[46] E. Neufeld and N. Kuster, "Platform for the modeling of *in vivo* effects relevant to implant em exposure safety," in *International Symposium on Electromagnetic Compatibility*, Tokyo, 2014.

[47] H. Pennes, "Analysis of tissue and arterial temperatures in the resting human forearm," *Journal of Applied Physiology*, vol. 1, no. 2, pp. 93-122, 1948.

[48] R. de Dear, "Convective and radiative heat transfer coefficients for individual human body segments," *International Journal of Biometeorology*, vol. 40, no. 3, pp. 141-156, 1997.

[49] P. Hasgall, F. Di Gennaro, C. Baumgartner, E. Neufeld, B. Lloyd, M. Gosselin, D. Payne, A. Klingenböck and N. Kuster, "IT'IS Database of thermal and thermomagnetic parameters of biological tissue. Version 4.0 May 15, 2018," IT'IS Foundation, Zurich, 2018.

[50] M. Jetté, K. Sidney and G. Blümchen, "Metabolic equivalents (METS) in exercise testing, exercise prescription, and evaluation of functional capacity," *Clinical Cardiology*, vol. 13, no. 8, pp. 555-565, 1990.

[51] D. Fourmet, B. Redortier and G. Havenith, "A method of whole-body skin temperature mapping in humans," *Thermology International*, vol. 2, no. 4, pp. 157-159, 2012.

[52] G. Tanda, "Total body skin temperature of runners during treadmill exercise," *Journal of Thermal Analysis and Calorimetry*, vol. 131, pp. 1967-1977, 2018.